Fatigue of extracted lead zirconate titanate multilayer actuators under unipolar high field electric cycling

Hong Wang, 1) Sung-Min Lee, James L. Wang, and Hua-Tay Lin

Materials Science and Technology Division, Oak Ridge National Laboratory,

Oak Ridge, TN 37831

#### **Abstract**

Testing of large prototype lead zirconate titanate (PZT) stacks presents substantial technical challenges to electronic testing systems, so an alternative approach that uses subunits extracted from prototypes has been pursued. Extracted 10-layer and 20-layer plate specimens were subjected to an electric cycle test under an electric field of 3.0/0.0 kV/mm, 100 Hz to 10<sup>8</sup> cycles. The effects of measurement field level and stack size (number of PZT layers) on the fatigue responses of piezoelectric and dielectric coefficients were observed. On-line monitoring permitted examination of the fatigue response of the PZT stacks. The fatigue rate (based on online monitoring) and the fatigue index (based on the conductance spectrum from impedance measurement or small signal measurement) were developed to quantify the fatigue status of the PZT stacks. The controlling fatigue mechanism was analyzed against the fatigue observations. The data presented can serve as input to design optimization of PZT stacks and to operation optimization in critical applications such as piezoelectric fuel injectors in heavy-duty diesel engines.

\_

<sup>1)</sup> Corresponding author. Tel: 1-865-574-5601; Fax: 1-865-574-6098; email: wangh@ornl.gov

# 1 Introduction

Lead zirconate titanate [PZT, Pb(Zr, Ti)O<sub>3</sub>] multilayer actuators are used in a broad range of applications that involve a working condition with high electric field. Among them are engine fuel injectors, servo displacement positioners, and vibration suppressors. <sup>1-3</sup> Improvements in the design and fabrication of modern PZT stacks have enabled the use of high electric fields, but such fields also cause increased tensile stress related to mismatched strains, increased dynamic overshoot in unloading, enhanced field concentration near the active—inactive transitional zone, and increased piezoelectric and dielectric hysteresis. <sup>4,5,6,7</sup> These changes raise significant concerns about fatigue and failure in PZT stacks.

Although the fatigue responses of bulk PZT<sup>8,9</sup> and PZT films<sup>10,11,12</sup> have been studied extensively, fatigue data on PZT stacks are limited. This is partly because a PZT stack typically has a multilayer configuration and composite structure, and the characterization of such a complicated system presents substantial technical challenges. Currently, fatigue testing of PZT actuators is mostly application-based and follows the procedure established for bulk PZT materials. For PZT actuators targeting applications using an ac field, fatigue evaluation is carried out through electric cycle tests using a defined waveform. The piezoelectric response or stroke of the stack under test is usually measured under quasi-static loading characterized by a low frequency and high electric field; the dielectric response is obtained from standard capacitance measurement with a capacitance meter at 1 kHz and 1 V.<sup>13</sup> The stroke and capacitance data obtained characterize the fatigue response of stacks to a certain degree, but these data should be used cautiously in applications because the working condition of PZT stacks may be different from that used in measurements. In a study conducted by Chaplya et al., <sup>14</sup> five commercial PZT stacks were tested under a rated electrical field in semi-bipolar mode, and stack fatigue was

characterized mainly in terms of mechanical strain. The fatigue performance of the PZT stacks was found to be related to the mechanical preload. A protocol for PZT stack fatigue testing was proposed recently by the authors of this paper that involves periodic measurements in cyclic process. The piezoelectric and dielectric data of PZT stacks were acquired in the same measurement session. Measurement conditions were defined according to application requirements.

Lengthy experimental work for a cycle test is usually necessary to obtain a set of test data equivalent to the lifetime of a regular product, more than 10<sup>9</sup> cycles. A multiple of the rated voltage can be used to accelerate fatigue testing in order to investigate the controlling mechanism of fatigue in a laboratory-feasible time scale. In fatigue tests with a field range of +4.5 to -0.9 kV/mm and a 20 MPa preload, a reduction of more than 40% was observed in mechanical strain, charge density, and hysteresis after 10<sup>8</sup> cycles. <sup>16</sup> Partial discharges, delaminations, micro-flaws, and etch grooves were found to result from fatigue. Charge defects (defect agglomerates)<sup>17</sup> and micro-flaws are believed to be responsible for steady degradation in stack performance, whereas partial discharges and delamination are more responsible for abrupt changes in cycling. Among these mechanisms, partial discharge is dynamically associated with the cycling process. However, this effect mainly arises from the surrounding medium as a result of the boundary condition and needs to be decoupled from the fatigue mechanisms inherently related to the stacks.

More recently, a fatigue test of commercial PZT stacks was conducted under high electric field within the surrounding medium provided by the electron fluid FC-40. No dielectric breakdown from partial discharge was observed, even though the testing field level had been driven to 6.0 kV/mm. The inherent degradation mechanisms responsible for electric fatigue and PZT stack failure were isolated. Apparently, only PZT stacks with limited capacitance can be

driven to such a high electric field; driving large-size stacks with several tens of microfarads to high electric field presents a significant technical challenge to the electronics.

The objective of this study is to develop an alternative approach to testing large PZT stacks by using extracted multilayer actuators. The extracted actuators are subunits of a prototype stack, consisting of 10 or 20 PZT layers. The internal and external electrodes of the extracted specimens were preserved and, therefore, can be used in the proposed electric cycle test. The extracted PZT actuators were tested under a unipolar high-level electric field and characterized accordingly. The following sections present the experimental technique, testing results, and related discussions.

# 2 Experimental Technique

#### 2.1 Material

Two groups of specimens, 10-layer and 20-layer PZT plates, were supplied by Cummins, Inc. (Columbus, IN). The specimens had a nominal plane size of  $11.5\times11.5$  mm. The nominal thicknesses of 10-layer and 20-layer specimens were 0.829 mm and 1.466 mm, respectively. The PZT layers were made of piezoceramic with properties close to those of PZT-5A. The PZT material is characterized by high Curie temperature and high piezoelectric coefficients, and has promising applications in fuel injection systems for diesel engines. The plate specimens were extracted from prototype stacks manufactured by EPCOS (Deutschlandsberg, Austria). The original stack size was  $11.5\times11.5\times54.0$  mm, the rated capacitance was  $16.15~\mu\text{F}$ , and the rated voltage was 160~V.

The PZT stacks have a modified plate-through open internal electrode configuration. Each internal electrode layer covers the entire surface of a PZT layer, except for one square corner

sized approximately  $300\times300$  µm. The corner area is reserved for external electrode of opposite sign. Specimens with sound surface integrity were selected and wired for the electric cycle tests in accordance with this study's dedicated procedure.

## 2.2 Testing setup

The main features of the electric cycle test setup or piezodilatometer can be found elsewhere. <sup>20,21</sup> The specimen was set vertically with one of the nontermination sides on the seat. The two termination sides were set aside, with wires connected to the high voltage (HV) and ground cables, respectively. The specimen was stabilized horizontally by a steel rod with a hemispherical head and a three-ball contact preloaded by a light-duty compression spring. An HV amplifier (±400 mA, 2 kV, Trek PZD-2000A, Medina, NY) was used to drive the specimen. The amplifier was equipped with both voltage and current monitoring channels. The latter were used in evaluating the dielectric response of the PZT actuator. As a result, electric field E<sub>3</sub> was applied in the thickness direction and dielectric response  $\varepsilon_{33}$  was measured. A linear variable capacitance transducer (L1-5 Measuretron, Inc., Butler, PA) was used to measure displacement of the specimen in the vertical direction, or the  $d_{31}$  piezoelectric response, with a signal conditioner (Model 33 Applied Test Systems, Inc., Butler, PA). The d<sub>31</sub> response is used because the displacement is much larger in the vertical direction than in the thickness due to the large side-to-thickness ratio of the PZT layers. Hence, the d<sub>31</sub> measurement is more accurate than that of  $d_{33}$ ; because both the  $d_{33}$  and  $d_{31}$  responses stem from the same polarization,  $^{21}$  the piezoelectric fatigue of the PZT device can be equivalently evaluated. The setup was hosted in a container filled with FC-40 (3M Company, St. Paul, MN) in order to prevent potential partial discharge during cycling. Testing control and data acquisition were achieved with LabView software along with a data acquisition board (NI USB-6251, Austin, TX).

## 2.3 Testing procedure

The as-received condition of an extracted and wired PZT specimen was evaluated first by impedance analysis. The test procedure was the same as that integrated into the cycle test, as described in the following. The capacitance *C* and resistance *R* of extracted PZT specimens were thus obtained.

Each specimen was tested under electric cyclic loading. A unipolar sine wave with peak field 3.0/0.0 kV/mm was used at 100 Hz with a total cycle number of up to 10<sup>8</sup>. Three 10-layer specimens and four 20-layer specimens were tested in this study.

Unless the specimen failed, the cycling process was interrupted to perform the measurements at a specific number of cycles:  $10^{0}$ ,  $10^{3}$ ,  $10^{5}$ ,  $10^{6}$ ,  $10^{7}$ ,  $3\times10^{7}$ ,  $8\times10^{7}$ , and  $10^{8}$ . Unipolar large signal measurement was conducted through two waveforms: a 0.1 Hz triangular wave and a 50 Hz sine wave. The first waveform was designed to measure mechanical strain and the second waveform, electric displacement. This approach was also used in a previous study and is, in fact, a hybrid of the measurement methods developed for the single-layer PZT and the multilayer PZT stack. The measurements were conducted by using two peak fields, 1.5/0.0 and 3.0/0.0 kV/mm. For each session, a wait of one hour before measurement minimized the effect of cycling-induced heat. Specimens under measurement generally remained on the same test stage as in cycling.

The mechanical strain–electric field or  $S_1$ – $E_3$  loops were acquired in the 0.1 Hz measurement. The loop amplitude  $\Delta S_1$ , piezoelectric hysteresis  $U_{d1}$ , piezoelectric coefficient  $d_{31}$ , and piezoelectric loss tangent  $\tan\delta_{p31}$  could thus be defined. For the 50 Hz measurement, the charge density–electric field or  $D_3$ – $E_3$  loops were acquired. The loop amplitude  $\Delta D_3$ , dielectric

hysteresis  $U_{H3}$ , dielectric coefficient  $\epsilon_{33}$ , and loss tangent  $\tan \delta_{33}$  were thus obtained. The data processing methods for the measurements can be found elsewhere. <sup>15,16,21</sup>

On-line monitoring was enabled. The dielectric response ( $\varepsilon_{33}$ ) of the specimen was monitored, and 10 data blocks were acquired in each cycling session (e.g., from  $10^3$  to  $10^5$  cycles). On-line monitoring generated a large volume of information for the cycle tests, so the measurements can be verified and better understood.

At the beginning and end of a cycle test, the fatigue status of the specimens was tested and evaluated by impedance analysis. A Solartron 1260 impedance/gain-phase analyzer was used along with dielectric interface 1296 (Hampshire, UK). The value 50 mV ac was selected in the impedance analysis. The spectra were recorded in the frequency range 0.01 Hz to 500 kHz with a sampling rate of 20 points per decade. An RC parallel circuit was then used in curve-fitting Nyquist plots (plots of the imaginary part versus the real part of the impedance) and, again, capacitance *C* and resistance *R* values were reported.

After the fatigue tests, all specimens were examined with an optical microscope (Nikon Nomarski Measure Scope MM-11, Tokyo, Japan).

# 3 Experimental Results

# 3.1 Pre-fatigue condition

#### 3.1.1 Impedance measurement

Ten as-received extracted PZT stacks in each group of specimens were examined by impedance analysis. Capacitance *C* and resistance *R* were obtained as given in Table 1. A significant level of estimate error was seen in *R* due to the limited data points in the low

frequency range, corresponding to large standard deviations in both groups. The estimate error in *C* was low, and the mean values 165.0 and 260.5 nF were obtained for the 10-layer and 20-layer specimens, respectively.

Specimens over a wide range of resistances were selected in subsequent cycle tests. Each specimen was loaded by the measurement field condition, namely three cycles of 0.1 Hz triangle wave with peak field 3.0/0.0 kV/mm. The loading served as a poling treatment for the PZT stacks. After poling, impedance analysis was conducted on the specimens to establish the baselines for R and C.

Dielectric breakdown occurred on a couple of 10-layer and 20-layer specimens, and the subsequent discussions focus only on the specimens that sustained the poling treatment. The impedance analysis results of tested PZT stacks are listed in Table 2. In most cases, C exhibited a slight increase after the initial treatment, and, again, uncertainty existed in the R estimate as indicated by the high error percentage for several specimens.

#### 3.1.2 Large signal measurement

The piezoelectric responses of PZT specimens obtained by measurements as described above revealed a range of variation. The measurements were, therefore, averaged among each group. The prefatigue levels of mechanical strain ( $\Delta S_1$ ), piezoelectric hysteresis ( $U_{d1}$ ), piezoelectric coefficient ( $-d_{31}$ ), and piezoelectric loss tangent ( $\tan\delta_{p31}$ ) can be seen from the left side of curves at  $10^0$  cycle presented in Figs. 1 and 2.

With regard to piezoelectric coefficient, it can be seen that  $d_{31}$  for 10-layer specimens was approximately -167 pm/V at the 1.5 kV/mm measurement field. The  $d_{31}$  obtained for multilayer actuators is actually very close to that of a monolithic material, for example, NCE57 in the Noliac data sheet.<sup>22</sup> The piezoelectric loss tangent was still 0.22 at 1.5 kV/mm for 10-layer

specimens; it is apparently a little lower than that of multilayer actuators made of similar PZT material. <sup>16</sup> The discrepancy may be attributed to differences in actuator configurations and measurement conditions. Nevertheless, the integrity of specimens has been demonstrated as being preserved adequately in terms of the piezoelectric coefficient mentioned here and the dielectric coefficient discussed below, although the specimens were extracted from parent PZT stacks but not delivered as a standard product.

A detailed examination of data revealed several important phenomena:

- 1) The mechanical strains under high measurement field were substantially higher than those under lower fields as expected, disregarding the number of layers or stack size.
- 2) The stack size effect on mechanical strain was obvious. A large stack size signified smaller mechanical strain under a given mechanical strain. But the stack size effect was less than that of measurement fields in the tested range.
- 3) Given a stack size (e.g., a 10-layer specimen), a high measurement field corresponded to a low value of  $-d_{31}$ , and also a lowered loss tangent. The measurement field effect was similar in both stack sizes.
- 4) The stack size effect was demonstrated on the piezoelectric coefficient. The 20-layer stacks delivered a relatively low coefficient compared to 10-layer stacks.

The pre-fatigue levels of dielectric response can be seen from the left side of curves at 10<sup>0</sup> cycle presented in Figs. 3 and 4. The maximum dielectric coefficient was obtained at 1.5 kV/mm for 10-layer specimens; it was approximately 15 nF/m, or relative dielectric constant 1690. The dielectric coefficient obtained for multilayer actuators was a little lower than that of bulk material such as NCE57 but was in the same range as multilayer actuators made of similar PZT materials of different geometries and different internal electrode configurations. <sup>16</sup> On the other

hand, the loss tangent 0.175 obtained at 1.5 kV/mm for 10-layer specimens was also very close to the data generated by Heinzmann et al.<sup>23</sup> and Wang et al.<sup>16</sup> for multilayer actuators made of similar PZT material. A detailed examination of data revealed dielectric responses similar to piezoelectric ones in terms of effects of measurement field level and stack size. Particularly, it has been observed that

- The stack size effect was much more significant than the effect of measurement field on dielectric coefficient.
- 2) Dielectric loss tangents were in the same range of piezoelectric loss tangent. Similar to the case of piezoelectric loss tangent, a higher measurement field resulted in a lower loss tangent. But a larger stack size corresponded to a higher loss tangent.

## 3.2 Piezoelectric fatigue response in large signal measurement

Dielectric breakdown occurred in two 10-layer (at  $1.6 \times 10^6$  cycles in P1007,  $6.5 \times 10^6$  cycles in P1009) and one 20-layer (at  $10^5$  cycles in P2010) specimens during the cycle tests. One 10-layer (P1002) and three 20-layer (P2005, P2007, P2011) specimens sustained  $10^8$  high-field electric cycles. In the following discussion, piezoelectric and dielectric fatigue responses from measurements were averaged among all the specimens in each group.

Given the effects of measurement field and stack size as described above, the effect of fatigue on mechanical strain and piezoelectric hysteresis is significant as can be seen in Fig. 1. It is observed that the fatigue curves (variation of strain versus number of cycles) in two measurement fields tended to become closer for each group toward the end of cycle tests.

The two groups exhibited little difference in fatigue response within the tested range. In the 10-layer, nonfatigue or slow fatigue was followed by rapid fatigue near 10<sup>5</sup> cycles, as seen by the 3.0 kV/mm measurement field. In the 20-layer, rapid fatigue appeared immediately after the start

of testing, and then a short stage of stabilization occurred around  $10^7$  cycles followed by a recovery stage around  $5\times10^7$  cycles. The 1.5 kV/mm measurements revealed a smaller level of variation due to the lower prefatigue response. In contrast, the fatigue curves of piezoelectric hysteresis  $U_{d1}$  generally showed a decreasing trend, except in 10-layer specimens at 1.5 kV/mm where a large loop area developed.

The variation of piezoelectric coefficient and loss tangent with number of cycles stemmed from the change in strain and piezoelectric hysteresis as seen in Fig. 2. However, the scenario is a little bit different. Besides the lower piezoelectric response at higher measurement field, the effect of stack size or number of layers on the fatigue response emerged to be more conspicuous. The recovery observed for 10-layer specimens is impressive in contrast to the fatigue in 20-layer specimens around 10<sup>3</sup> to 10<sup>5</sup> cycles. As a result of that, the fatigue curves of the two groups separated and then converged in the late stage of the cycle tests. Overall, fatigue-induced variation on piezoelectric loss tangent was quite limited, while the 1.5 kV/mm measurement for the 10-layer was exceptional. A rapid increase in loss tangent was observed from measurement field 1.5 kV/mm around 10<sup>6</sup> cycles, corresponding to the increase in piezoelectric hysteresis as shown in Fig. 1.

The normalized piezoelectric coefficient and shifted loss tangent with respect to prefatigue level for all cases of stack size and measurement field are given in Fig. 5.

# 3.3 Dielectric fatigue response in large signal measurement

A slow fatigue stage can be identified for 10-layer specimens in both 1.5 and 3.0 kV/mm measurement fields before 10<sup>5</sup> cycles as shown in Fig. 3. The fatigue of 20-layer specimens appeared more linearly proportional to the logarithmic number of cycles, and the fatigue rates of charge density detected by the two measurement fields seemed quite similar. The effect of

fatigue on dieelctric hysteresis appeared to be similar in the 1.5 and 3.0 kV/mm measurements because the distance established for each group in prefatigue was almost maintained during the cycle tests.

Overall, the dielectric coefficient exhibited a decreasing trend with number of cycles as seen in Fig. 4. The slow fatigue or recovery stage can be seen for 10-layer specimens before 10<sup>5</sup> cycles, and the logarithmic linearity was more developed in the case of 20-layers. The difference between the 1.5 and 3.0 kV/mm measurement fields diminished towards the end of the cycle tests, even though the difference due to stack size was still significant. The variation of loss tangent was again limited; most of the loss tangents exhibited a decreased value at 10<sup>8</sup> cycles, except the 3.0 kV/mm measurement for 10-layer specimens.

The normalized dielectric coefficient and shifted loss tangent with respect to pre-fatigue levels are shown in Fig. 6. A deceasing trend was seen in the normalized coefficient in all cases evaluated. Disregarding stack size, a larger decrease was generally obtained at 1.5 kV/mm than at 3.0 kV/mm. The degree of variation in shifted loss tangent, overall, was limited and smaller than that of piezoelectric loss tangent as seen in Fig. 5.

# 3.4 Dielectric fatigue response in on-line monitoring

The dielectric responses based on on-line monitoring are given in Fig. 7 (a) and (b) for a 10-layer (P1002) and a 20-layer (P2007) stack, respectively. It is worthwhile noting that the responses were actually obtained with applied electric field 3.0 kV/mm at 100 Hz. The first data point of each cycle session was not used in the plots due to the transient property of loading.

The dielectric coefficient for both specimens fluctuated but overall showed a defined decreasing trend. Similar to the measurements in Section 3.3, the dielectric coefficient in larger stacks was again lower than that in smaller stacks. A detailed investigation revealed that

discontinuous variations were typically associated with interruptions occurring during measurement. Such interruptions caused the subsequent cycle session to display either a positive or a negative effect on dielectric coefficient. Local increases in monitored dielectric coefficient corresponded to periods in which recoveries occurred in the measured piezoelectric and dielectric responses as seen in Figs. 2 and 4. An oscillatory response was also seen in the loss tangent, although the trend was not as appreciable as in the dielectric coefficient.

## 3.5 Impedance response

The impedance analysis was integrated into the fatigue evaluation of PZT stacks. Curvefitting using RC parallel circuit demonstrated that capacitance C indeed decreased near the end of cycle testing whereas resistance R did not, as seen in Table 2.

#### 4 Discussion

#### 4.1 Electric measurement field effect

A higher measurement field did not result in a higher piezoelectric or dielectric coefficient, although a higher mechanical strain and charge density were obtained. With the electric field over two times the coercive field in 0.1 Hz hysteresis measurement, domain switching becomes increasingly saturated and so does polarization. Both the D-E and S-E loops bent towards the E axis with increasing electric field. The tendency of downward bending at high field measurements was also seen in multilayer actuator made of PZT-5H<sup>15</sup> and bulk PZT with a high rhombohedral phase content.<sup>24</sup> Because the strain and electric displacement could not increase proportionally, piezoelectric and dielectric coefficients would decrease with increasing electric field. Apparently, the fatigue resulted in reduced domain switching and more downward bending

of the S-E loop at the high field end. This corresponds to a larger increase in normalized piezoelectric coefficient at the 3.0 kV/mm measurement than at 1.5 kV/mm (Fig. 5).

Unipolar loading in 50 Hz dielectric measurement can be simply decomposed into a dc part and an ac part; the amplitude of each component was half of the original amplitude. The dc bias field has a substantial effect on domain activity because it stabilizes the domain so as to limit domain wall motion and domain switching. This has been validated by small-signal measurements in which reversible domain motion becomes very difficult at the high dc bias field; both piezoelectric and dielectric coefficients decreased with increasing dc field. 17,25 When the applied ac field entered the Rayleigh region, domain switching was suppressed by dc bias in both dielectric and piezoelectric coefficients. <sup>26,7</sup> Because the dielectric coefficient itself decreases with increasing dc bias or increasing measurement field, the dielectric measurement at 1.5 kV/mm exhibited more decrease in normalized dielectric coefficient (Fig. 6) than at 3.0 kV/mm. At 1.5 kV/mm, the proportion of domain switching (other parts are ionic contribution and reversible domain motion) to the overall dielectric response was apparently higher than that at 3.0 kV/mm, corresponding to the larger value of loss tangent (Fig. 4). Domain switching was quite sensitive to fatigue, with a greater extent of decrease seen at 1.5 kV/mm. This is a little different from that <sup>17</sup> obtained with smaller measurements in which the fatigueinduced relative decrease in  $\epsilon_{33}$  at  $E_{max}=2.0~kV/mm$  is larger than at E=0~kV/mm. The smaller signal measurement generally involved reversible domain wall motion, whereas in this study an electric field greater than 1.5 kV/mm mobilized irreversible domain motion from domain switching.

## 4.2 Stack size effect on fatigue

A stack size effect (in terms of number of layers) was observed on both piezoelectric and dielectric response, as seen from large signal measurements in Figs. 2 and 4. Given a measurement field, large stacks typically had a relative low value of  $-d_{31}$  or  $\varepsilon_{33}$ . Such size effect was also reflected in capacitance C measured by the impedance analyzer, in which the 10-layer and 20-layer stacks were found to have 165.0 and 260.5 nF, respectively. Namely, capacitance did not scale up with stack size owing to the size effect of the dielectric coefficient.

The size effect on piezoelectric and dielectric responses is quite similar to that on mechanical strength in structural ceramic materials. The size effect is believed to stem from the volume flaws that dominate the piezoelectric and/or dielectric response of PZT. The flaws serve as field concentrators<sup>27,28</sup> within a stressed body under mechanical or electric loading and cause local damage and local dielectric breakdown. Such flaws in PZT layers are inherently related to the PZT sintering and poling process.<sup>29,30</sup> A large specimen containing a large population of structural flaws generally provides a greater probability of sampling a flaw, resulting in reduced electric responses. This partly explains the overall size effect on the piezoelectric and dielectric fatigue seen in Figs. 2 and 4.

Apparently, the size effect mechanism of fatigue in PZT stacks is more complicated than the volume flaws described in a mechanical system. The comprising PZT layers and metal electrodes generally possess different coefficients of thermal expansion and different dielectric/piezoelectric coefficients. Owing to these differences, the PZT layer and electrode deformed differently in the sintering, cooling, and poling processes, and restraining created residual stress upon process completion. The residual stress modified the mechanical stress state within the PZT layer near the electrode. A nearby electrode layer can, therefore, emerge

mechanically modified or degraded. It has been pointed out<sup>31</sup> that stress in PZT films resulting from nonpiezoelectric substrate could be high enough to induce mechanical fatigue. The nearby electrode layer may appear as a degraded dielectric layer as reviewed by Tagantsev et al. in a related reference.<sup>10</sup> A direct impact of polarization fatigue is the reduced dielectric coefficients in PZT materials.<sup>8,9,10,11</sup> Luo and Wang<sup>12</sup> demonstrated that, in fatigued PZT film, degraded dielectric layers also tend to increase under unipolar cycling. Under unipolar high-electric-field cycling, a nearby electrode layer that is degraded mechanically and electrically could form and evolve during cycling, controlling the piezoelectric and dielectric fatigue of the PZT layer. Again, a large PZT stack containing a large number of electrode–PZT interfaces provides greater probability of sampling a degraded nearby electrode layer. This is an additional explanation of the size effect on piezoelectric and dielectric fatigue as observed in Figs. 2 and 4.

Given a measurement field, the normalized dielectric coefficient ( $\varepsilon_{33}/\varepsilon_{330}$ ) showed a similar degree of reduction between 10- and 20-layer specimens during cycling (Fig. 6). The normalized piezoelectric coefficient ( $d_{31}/d_{310}$ , Fig. 5), on the other hand, exhibited a little different scenario. Particularly, a much larger reduction was observed in 20-layer specimens than in 10-layer specimens, even though both merged at  $10^8$  cycles. Obviously, electro-mechanical coupling in the PZT stack substantially degraded as the volume of damage in nearby electrode layers increasingly developed. Namely, a PZT stack with a larger number of PZT layers (i.e., a larger number of PZT-electrode interfaces) corresponds to a more fatigued piezoelectric response but not necessarily to an equally reduced dielectric response.

Delamination at the PZT-electrode interface would occur should the interface strength be reached. Delamination has been strongly associated with fatigue and failure of commercial PZT stacks. Optical microscopy performed on the extracted PZT stacks tested in this study

revealed that for those experiencing dielectric breakdown, extended burning was usually related to PZT-electrode interfaces.

#### 4.3 On-line monitoring, fatigue rate, and fatigue index

The measurement process had a certain amount of effect on fatigue, as seen in discontinuous changes in dielectric response from the on-line monitoring (3.0 kV/mm 100 Hz, Fig. 7). In P1002, discontinuous changes in  $\varepsilon_{33}$  were observed at measurement interrupts at cycle numbers  $10^3$ ,  $10^5$ ,  $10^6$ , etc. At  $10^3$ , an abrupt increase was observed after measurement taking. The high electric field in measurement apparently re-poled the fatigued PZT and caused the dielectric coefficient to recover. At 10<sup>5</sup>, the effect of measurement was associated with a slight drop, and the measurement steps seemed to be part of the cyclic fatigue. It is worthwhile noting that the discontinuous increase was also related to interruptions not associated with measurements, particularly in P2007 at  $5\times10^7$  cycles. The abrupt increase following an interruption is quite similar to the strain recovery of the PI-LV stack after testing under 1.20/-0.24 kV/mm at 40 Hz for  $10^7$  cycles. <sup>14</sup> Cycling-induced self-heating in that PZT stack was responsible for the strain decrease, and subsequent cooling was observed to account for strain recovery. However, the effect of self-heating on strain was seemingly related to the structure of the PI-LV PZT stack because other PZT stacks demonstrated various degrees of strain increase during cycling. It remains to be investigated if the self-heating is related to a transient response in extracted PZT stacks.

Although the local fluctuations in dielectric coefficient were impressive, a decreasing trend was well defined, as can be seen in Fig. 8. A linear regression analysis was conducted on all specimens that had a complete time series on  $\varepsilon_{33}$ , with the following expression,

$$\varepsilon_{33} = b_0 + b_1 \log(N), \tag{1}$$

where N is the number of cycles, and  $b_0$ ,  $b_1$  are curve-fitting parameters measuring the initial  $\varepsilon_{33}$  and degradation rate. The results are given in Table 3. Based on the time series upon  $10^8$  cycles, the degradation rate of  $\varepsilon_{33}$  of the PZT stacks was found to be 0.19 to 0.36 nF per decade of cycles. The degradation rate should be related to the testing condition, and the discussion is thus limited to cyclic testing under 3.0 kV/mm 100 Hz.

The degradation of piezoelectric or dielectric coefficient signifies that PZT stack performance can be monitored. Although capacitance responded to PZT stack degradation along with number of accumulated cycles, the sensitivity was low and uncertainty was exhibited by the variation of capacitance. An alternative is pursued here by considering the spectrum of the real part of admittance *Y* in a defined frequency range.

$$Y = I/V \text{ or } Y = G + jB \tag{2}$$

where I is the current, V the voltage,  $G = \operatorname{real}(Y)$  the conductance, and  $B = \operatorname{imag}(Y)$  the susceptance. The approach is widely used in electro-mechanical impedance analysis for structural health monitoring and has been demonstrated to be quite effective.  $^{32,33,34}$  A statistical parameter is generally required to quantify the variation of spectrum; monitoring of the parameter provides information on the status of structural health. For fatigue, the statistical parameter or fatigue index can be defined by RMSD (root mean square deviation) as follows.

$$RMSD(\%) = \sqrt{\frac{\sum_{i=1}^{N} (G_i^1 - G_i^0)^2}{\sum_{i=1}^{N} (G_i^0)^2}} \times 100$$
(3)

where  $G_i^1$  is the post-fatigue conductance at the i<sup>th</sup> measurement point,  $G_i^0$  is the corresponding pre-fatigue value, and summation is taken over the frequency range. In typical practice, a frequency range with a sufficient number of peaks to generate the desired measurement is selected. The conductance spectra, real(Y), of the 10-layer (P1002) and the 20-layer (P2007) were obtained by converting the impedance signature in the frequency range 10 to 500 kHz and are presented in Fig. 9. Two plots in each figure correspond to 10<sup>0</sup> and 10<sup>8</sup> cycles, with the former serving as a baseline. An anti-resonant frequency (at which the admittance is minimized) is seen around 170 kHz, corresponding to the extensional mode of the actuator due to the d<sub>31</sub> effect. 18 The RMSD based on Eq. (3) was evaluated for four specimens having a complete impedance data set, and was further correlated to the relative change in the on-line monitoringbased dielectric coefficient. The RMSD was shown to be well correlated to the relative change of  $\varepsilon_{33}$ , as illustrated in Fig. 10. The evaluation of dielectric coefficient made use of the prediction based on Eq. (1). Monitoring of PZT stacks based on the fatigue index has thus been demonstrated to be promising in several respects. First, the excitation voltage used in measurement is quite low, so the measurement itself has little impact on PZT stack performance. Second, measurement focuses on a selected frequency range instead of a wide range of frequency (from several mHz to MHz as in impedance analysis), and data acquisition can be faster and more reliable. The data discussed above were limited to the pre-fatigue and postfatigue, and the suggested RMSD-based fatigue index remains to be correlated with the data during the fatigue process.

## 4.4 Fatigue mechanism

Different fatigue responses in piezoelectric and dielectric coefficients were also seen in the PZT-5H stack under mechanical preload<sup>15</sup>; 6% and 10% decreases were observed in normalized piezoelectric and dielectric coefficients, respectively. Small signal measurement (at E<sub>max</sub> = 2.0 kV/mm)<sup>17</sup> and large signal measurement<sup>21</sup> also revealed a larger decrease in dielectric coefficient than in piezoelectric coefficient in bulk PZT. Obviously, the stronger dielectric fatigue in these previous studies is different from that in the current study in which a greater piezoelectric fatigue was observed. It should be stressed that a commensurate reduction in dielectric and piezoelectric coefficients was actually observed in cyclic fatigue of PZT stacks made of similar PZT material but a different internal electrode configuration.<sup>16</sup> Delamination in those stacks and partial discharge on the surface of the stacks made a significant contribution to the greater than 40% reduction in piezoelectric and dielectric coefficients.

The intrinsic piezoelectric  $d_{31}$  and dielectric  $\epsilon_{33}$  responses can be related to electrostrictive coefficient  $Q_{ij}$  and spontaneous polarization  $P_s$  as follows.<sup>36</sup>

$$d_{31} = 2\varepsilon_{33}Q_{12}P_s \tag{4}$$

This relation is derived from single-domain activity in which spontaneous  $P_s$  is in the direction X3, can generally be valid for ceramics, and can be substituted by instantaneous polarization P. The electrostrictive coefficient  $Q_{12}$  is quite independent of temperature, frequency, and fatigue treatment.<sup>37</sup> With this in mind, Eq. (4) can be rewritten in terms of quantities normalized to prefatigue values:

$$\frac{d_{31}}{d_{310}} = \frac{\varepsilon_{33}}{\varepsilon_{330}} \cdot \frac{P}{P_0} \tag{5}$$

The use of Eq. (4) is limited to cases not involving large-scale domain switching. Thus, Eq. (4) measures the contributions of intrinsic and small-scale domain switching parts to the piezoelectric coefficient. Let us consider the moment at  $10^7$  cycles with focus on 20-layer at 3.0 kV/mm measurement. P/P<sub>0</sub> was about 0.91 if estimated by the normalized charge density  $(\Delta D_3/\Delta D_{30} \text{ in Fig. 3})$ , and  $\varepsilon_{33}/\varepsilon_{330}$  was at the similar level 0.92 (Fig. 6) if based on large signal measurement. A value of 0.83 in the normalized piezoelectric coefficient can be predicted according to Eq. (5), which was lower than 0.70 as observed at that moment (Fig. 5).

The observation demonstrated that fatigue from the piezoelectric response of the PZT stack is greater than fatigue from the ionic contribution and reversible domain wall motion. Additional fatigue is attributed to irreversible wall activity with domain switching.

Domain switching itself constitutes the majority of mechanical strain and, at the same time, serves as the driving force to polarization fatigue. The domain switching under a unipolar electric field is controlled by the depolarization that manipulates the switch and back-switch during the first and second half of the cycle.  $^{12}$  Back-switching during unipolar fatigue is defined as a polarization switching process driven by the residual depolarization field,  $E_{dep}(t) - E_{appl}(t)$ , when the applied unipolar field  $E_{appl}$  is smaller than  $E_{dep}$ , and it occurs in the direction opposite that of  $E_{appl}$ . Similarly, switching during unipolar fatigue is defined as a polarization switching process driven by the residual applied field,  $E_{appl}(t) - E_{dep}(t)$ , when  $E_{appl}$  is larger than  $E_{dep}$ , and it occurs in the same direction as that of  $E_{appl}$ . The switching and back-switching change over when  $E_{appl}$  varies relative to  $E_{dep}$ . The repetitive switching and back-switching process eventually leads

to unipolar fatigue, corresponding to the less switchable polarization estimated by instantaneous polarization in Eq. (5). Domain wall pinning is responsible for the reduced switchability as described extensively. <sup>8,10,38</sup> Micro defects such as pores, cracks, and even triple-point boundaries can serve as reservoirs of charge carriers that eventually clamp the domain walls.

The extrinsic part of the piezoelectric coefficient is attributed merely to non-180° domain wall motion. <sup>39</sup> The fatigue-induced reduction in domain switching as discussed above has a direct impact on the extrinsic part, which corresponds to a reduced value of piezoelectric coefficient in large signal measurement. Moreover, domain switching strain in a polycrystalline PZT ceramic is influenced by the stress–strain interaction between adjacent parts because of misalignment of the crystallographic axes in the neighboring grains. Such interaction can be superimposed or modulated onto the basic mechanical strain and have various effects on the observed piezoelectric coefficient of bulk PZT. <sup>40</sup> As mentioned above, residual stress is inherently related to the PZT–electrode interface or nearby electrode layers in PZT stacks, and the extrinsic part of mechanical strain in PZT stacks can be limited by residual stress, depending on the number of layers. The stress state of the nearby electrode layers evolved with the number of accumulated cycles and modified the electro-mechanical coupling of the PZT stack, resulting in the more pronounced piezoelectric fatigue observed by large signal measurement.

Also realized was that different frequencies were used in the evaluation of piezoelectric and dielectric coefficients, namely 0.1 Hz versus 50 Hz, but the effect within the range of frequency is limited.<sup>41</sup>

#### 5 Conclusions

Testing and characterization of large prototype PZT stacks present substantial technical challenges to electronic testing systems. The work in this study showed that an alternative approach can be pursued by using subunits extracted from prototype stacks. Piezoelectric and dielectric integrity was maintained even though the PZT plate specimens experienced an additional loading process involved with the extraction after factory poling. Piezoelectric and dielectric properties comparable to those of standard products made of similar PZT materials can be attained. This observation should be limited to poling that involves unipolar electric loading.

Extracted 10-layer and 20-layer plate specimens were studied by use of an electric cycle test under an electric field of 3.0/0.0 kV/mm, 100 Hz to 10<sup>8</sup> cycles. Evaluation of the fatigue of piezoelectric and dielectric coefficients depended on the field level of the large signal measurement as a result of domain activities. The use of data generated at the electric field equivalent to that in cycling is recommended. Decreases of 25% and 10% were observed in piezoelectric and dielectric coefficients, respectively, after 10<sup>8</sup> cycles under 3.0/0.0 kV/mm, but the loss tangent varied to a limited extent. The residual stress of PZT–electrode interfacial layers and the evolution of the mechanical stress state, to a greater extent, account for the discrepancy and the related size effect of fatigue.

The piezoelectric and dielectric fatigue responses were related to the size of extracted PZT stacks or the number of PZT layers. The population of dominant flaws in active PZT volumes and the number of PZT–electrode interfacial layers in PZT stacks are responsible for the size effect. Additional tests are needed to confirm the observation and to further correlate the fatigue in the extracted PZT stacks to that of prototypes.

The degradation of piezoelectric and dielectric coefficients provides an effective tool for monitoring the status of PZT stacks in service, as demonstrated by the enabling on-line monitoring technique. Dielectric fatigue rate, 0.19 to 0.36 nF per decade of cycles, was defined for the extracted PZT stacks. The fatigue rate is limited to the tested range, and extrapolation of the observation to high numbers should be validated by fatigue testing beyond 10<sup>8</sup> cycles.

Examination of the fatigue status of PZT stacks with small signal measurement can be improved by using a statistical parameter of the spectrum defined over a specified frequency range. The RMSD (root mean square deviation) or fatigue index based on conductance had a well-defined linearity with the reduction in on-line monitoring-based dielectric coefficient. The fatigue index is adaptable to on-line monitoring also.

#### **ACKNOWLEDGEMENTS**

The authors are grateful to ORNL Curt Maxey and Jian Chen for reviewing the manuscript. The authors thank Dr. Michael Lance for his help in impedance measurement. This research was sponsored by the U.S. Department of Energy, Office of Energy Efficiency and Renewable Energy, Vehicle Technologies Program, Propulsion Materials Program under contract DE-AC05-00OR22725 with UT-Battelle, LLC.

#### References

<sup>1</sup> K. Uchino, Piezoelectric Actuators and Ultrasonic Motors (Boston, MA: Kluwer Academic, 1997).

- <sup>2</sup> C. Schuh, T. Steinkopff, A. Wolff, and K. Lubitz, Smart Structures and Materials 2000: Active Materials: Behavior and Mechanics (Newport Beach, CA, March 2000); Proc. SPIE 3992, 165.
  - <sup>3</sup> M. Mitrovic, G. P. Carman, and F. K. Straub, Int. J. Solids Struct. **38**, 4357 (2001).
  - <sup>4</sup> A. Furuta and K. Uchino, J. Am. Ceram. Soc. **76**, 1615 (1993).
- <sup>5</sup> K. Lubitz, C. Schuh, T. Steinkopff, and A. Wolff, in Piezoelectric Materials in Devices, edited by N. Setter (EPFL, Lausanne, Switzerland, 2002), p. 183.
- <sup>6</sup> U. Joshi, Y. Kalish, C. Savonen, V. Venugopal, and N. Henein, FY 2003 Progress Report, DOE program on Heavy Vehicle Propulsion Materials, p.7.
  - <sup>7</sup> D. A. Hall, J. Mater. Sci. **36**, 4575 (2001).
  - <sup>8</sup> D. C. Lupascu and J. Rödel, Adv. Eng. Mater. **7**, 882 (2005).
  - <sup>9</sup> J. Glaum, T. Granzow, L. A. Schmitt, H. J. Kleebe, J. Rödel, Acta Mater. **59**, 6083 (2011).
  - <sup>10</sup> A. K. Tagantsev, I. Stolichnov, E. L. Colla, and N. Setter, J. Appl. Phys. **90**, 1387 (2001).
  - <sup>11</sup> X. J. Lou, J. Appl. Phys. **105**, 024101 (2009).
  - <sup>12</sup> X. J. Lou and J. Wang, J. Appl. Phys. **108**, 034104 (2010).
- <sup>13</sup> B. Andersen, F. Jensen, and S. Ouchouche, Ninth Int. Conf. on New Actuators, 14–16 June, 2004, Bremen Germany, <a href="http://www.noliac.com">http://www.noliac.com</a>.
- <sup>14</sup> P. M. Chaplya, M. Mitrovic, G. P. Carman, and F. K. Straub, J. Appl. Phys. **100**, 124111 (2006).
  - <sup>15</sup> H. Wang, A. A. Wereszczak, and H.-T. Lin, J. Appl. Phys. **105**, 014112 (2009).
- <sup>16</sup> H. Wang, T. A. Cooper, H.-T. Lin, and A. A. Wereszczak, J. Appl. Phys. **108**, 084107 (2010).
  - <sup>17</sup> N. Balke, D. C. Lupascu, T. Granzow, and J. Rödel, J. Am. Ceram. Soc. **90**, 1081 (2007).
  - <sup>18</sup> F. W. Zeng, H. Wang, and H.-T. Lin, J. Appl. Phys. **114**, 024101 (2013).
- <sup>19</sup> C. A. Randall, A. Kelnberger, G. L. Yang, R. E. Eitel, T. R. Shrout, J. of Electroceramics **14**, 177 (2005).

- <sup>20</sup> H. Wang, A. A. Wereszczak, and H.-T. Lin, Dual-rod piezodilatometer and method for testing a piezoceramic plate, ORNL Invention Disclosure 200802179, US DOE S-115, 208.
- <sup>21</sup> H. Wang, T. Matsunaga, H.-T. Lin, and A. M. Mottern, Smart Mater. Struct. **21**, 025009 (2012).
  - <sup>22</sup> Noliac, Piezo Ceramics, 2012, http://www.noliac.com.
- <sup>23</sup> A. Heinzmann, E. Hennig, B. Kolle, D. Kopsch, S. Richter, H. Schwotzer, and E. Wehrsdorfer, Actuator 2002, also on http://www.pi-usa.us/technotes.html
  - <sup>24</sup> H. Kungl, T. Fett, S. Wagner, and M. J. Hoffmann, J. Appl. Phys. **101**, 044101 (2007).
- <sup>25</sup> Y. Zhang, D. C. Lupascu, E. Aulbach, I. S. Baturin, A. Bell, V. Y. Shur, and J. Rödel, Acta Mater. **53** 2203-13 (2005)
  - <sup>26</sup> V. Perrin, M. Troccaz, and P. Gonnard, J. Electroceramics 4 189 (1999).
  - <sup>27</sup> D. Wang, Y. Fotinich, and G. P. Carman, J. Appl. Phys. **83**, 5342 (1998).
  - <sup>28</sup> S.-J. Kim and Q. Jiang, Smart Mater. Struct. **5**, 321 (1996).
  - <sup>29</sup> H. T. Chung, B. C. Shih, and H. G. Kim, J. Am. Ceram. Soc. **72**, 327 (1989).
  - <sup>30</sup> K. Uchino, Acta Mater. **46**, 3745 (1998).
  - <sup>31</sup> K. Khachaturyan, J. Appl. Phys. **77**, 6449 (1995).
  - <sup>32</sup> C. Liang, F. P. Sun, and C. A. Rogers, J. Intell. Mater. Syst. and Struct. **5**, 12-20 (1994).
- <sup>33</sup> G. Park, H. Sohn, C. R. Farrar, and D. J. Inman, The Shock and Vibration Digest **35**, 451-463 (2003).
  - <sup>34</sup> V. G. M. Annamdas, and C. K. Soh, J. Intell. Mater. Syst. and Struct. **21**, 41-959 (2010).
- <sup>35</sup> V. Giurgiutiu, and C. A. Rogers, Smart Structures and Materials 1998: Smart Structures and Integrated Systems (San Diego, California, USA, March 1998); Proceedings of SPIE 3329, 536.
  - <sup>36</sup> A. F. Devonshire *Philos. Mag.* **42** 1065-79 (1951).

- <sup>37</sup> Q. M. Zhang, W. Y. Pan, S. J. Sang, and L. E. Cross, *J. Appl. Phys.* **64** 6445-51 (1988)
- <sup>38</sup> W. L. Warren, D. Dimos, B. A. Tuttle, G. E. Pike, R. W. Schwartz, P. J. Clews, and D. C. McIntyre, J. Appl. Phys. **77**, 6695 (1995).
  - <sup>39</sup> P. Chaplya and G. Carman, J. Appl. Phys., **92**, 1504 (2002).
- <sup>40</sup> H. Kungl, R. Theissmann, M. Knapp, C. Baehtz, H. Fuess, S. Wagner, T. Fett, and M. J. Hoffmann, Acta Mater. **55**, 1849 (2007).
  - <sup>41</sup> M. Demartin and D. Damjanovic, Appl. Phys. Lett. **68**, 3046 (1996).

# **List of Tables**

Table 1 Resistance and capacitance of as-received extracted PZT stacks  $^{\it a}$ 

Table 2 Variations of R and C values in cycle tests a

Table 3 Curve-fitting results based on on-line monitoring  $^a$ 

#### **List of Figures**

Figure 1(a) Mechanical strain and (b) piezoelectric hysteresis as a function of cycle number.

Figure 2(a) Piezoelectric coefficient and (b) loss tangent as a function of cycle number.

Figure 3(a) Charge density and (b) dielectric hysteresis as a function of cycle number.

Figure 4(a) Dielectric coefficient and (b) loss tangent as a function of cycle number.

Figure 5(a) Normalized piezoelectric coefficient and (d) shifted piezoelectric loss tangent as a function of cycle number.

Figure 6(a) Normalized dielectric coefficient and (d) shifted loss tangent as a function of cycle number.

Figure 7 Dielectric coefficient and loss tangent as a function of cycle number based on online monitoring for (a) a 10-layer specimen and (b) a 20-layer specimen.

Figure 8 Dielectric coefficient and curve fitting as a function of cycle number based on online monitoring for (a) a 10-layer specimen and (b) a 20-layer specimen.

Figure 9 Spectrum of admittance real part (Y) as a function of cycle number for (a) a 10-layer specimen and (b) a 20-layer specimen.

Figure 10 Correlation of relative change of  $\epsilon_{33}$  to RMSD. Test results are based on on-line monitoring for both 10- and 20- layer specimens.

Table 1 Resistance and capacitance of as-received extracted PZT stacks  $^a$ 

Specimen configuration	C (nF)		R (Mohm)		Number of
	Mean	Std. dev.	Mean	Std. dev.	specimens
10-layer	165.0	10.4	1,044.6	619.3	10
20-layer	260.5	22.8	514.5	295.4	10

 $<sup>^</sup>a$  Parallel RC circuit: 100 K ~ 0.10 Hz

Table 2 Variations of R and C values in cycle tests a

Specimen	Condition b	Capacitance	Estimate	Resistance	Estimate
		(nF)	error (%)	(Mohm)	error (%)
P1002	Before poling	176.5	0.86	23.2	2.70
	After poling	191.8	0.52	46.0	2.30
	1.0×10 <sup>8</sup>	166.9	0.32	1,500.0	3.00
P1007	Before poling	175.0	0.37	215.0	4.90
	1.6×10 <sup>6</sup> c				
P1009	Before poling	176.0	0.33	1,870.0	36.30
	6.5×10 <sup>6</sup> c				
P2005	Before poling	276.5	0.49	572.0	26.00
	After poling	296.3	0.56	942.0	52.80
	$3.0 \times 10^7$	280.0	0.51	500.0	24.20
	1.0×10 <sup>8</sup>	269.4	0.40	765.0	27.90
P2007	Before cycling	242.0	0.40	873.0	27.8
	After poling	255.4	0.40	94.4	36.70
	1.0×10 <sup>8</sup>	227.3	0.40	160.0	50.00
P2010	Before poling	293.9	1.10	37.5	5.40
	After poling	285.4	0.65	182.0	11.60
	1.0×10 <sup>5 c</sup>	245.1	0.47	0.4	0.54
P2011	Before poling	285.1	0.39	971.0	36.70
	After poling	293.8	0.73	1,350.0	58.10
	1.0×10 <sup>8</sup>	262.7	0.36	505.0	16.30

<sup>&</sup>lt;sup>a</sup> Fitting range: 100 K - 0.01/0.10 Hz.

<sup>&</sup>lt;sup>b</sup> Poling condition: 3.0/0.0 kV/mm, 0.1 Hz, 3 cycles

<sup>&</sup>lt;sup>c</sup> Dielectric breakdown observed.

Table 3 Curve-fitting results based on on-line monitoring  $^a$ 

Specimen	b <sub>1</sub>	$b_0$ , $\varepsilon_{33}(N=10^0)$	$\epsilon_{33}(N=10^8)$
	nF/decade	nF	nF
1002	-0.242	13.956	12.025
2005	-0.186	12.278	10.794
2007	-0.347	11.292	8.519
2011	-0.359	12.814	9.939

<sup>&</sup>lt;sup>a</sup> Eq. (1) used  $\varepsilon_{33} = b_0 + b_1 * \log(N)$ .

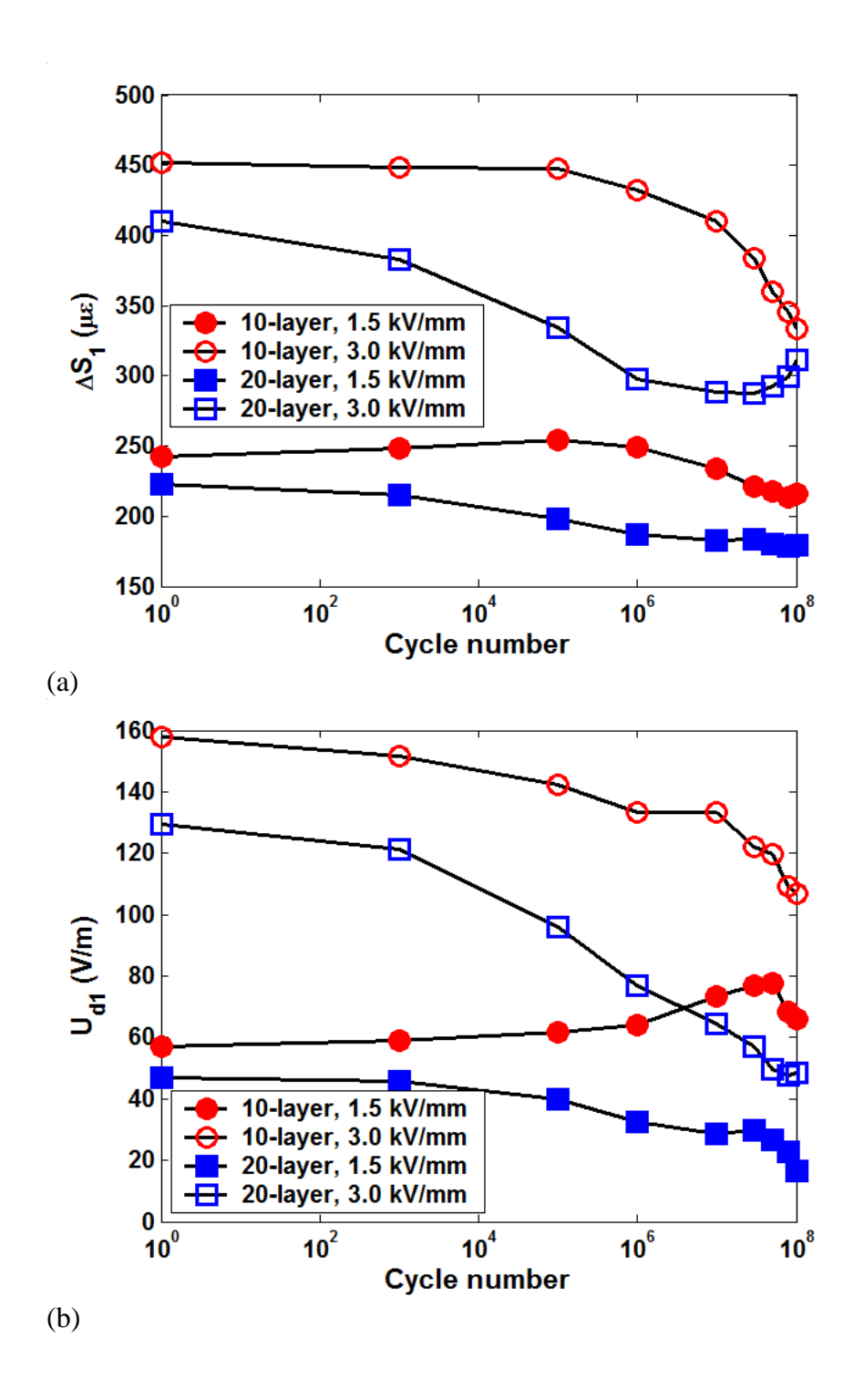


Figure 1(a) Mechanical strain and (b) piezoelectric hysteresis as a function of cycle number.

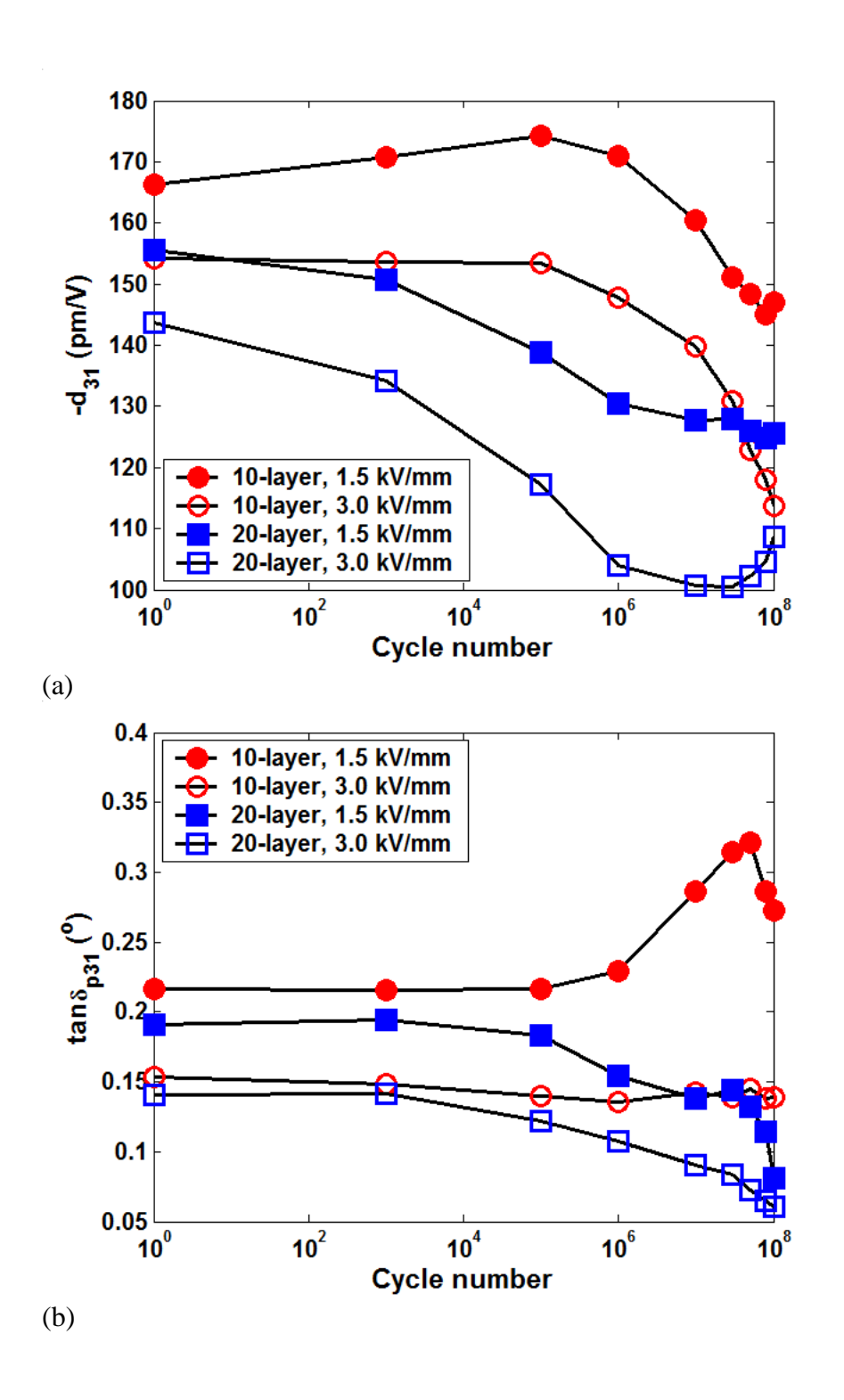


Figure 2(a) Piezoelectric coefficient and (b) loss tangent as a function of cycle number.

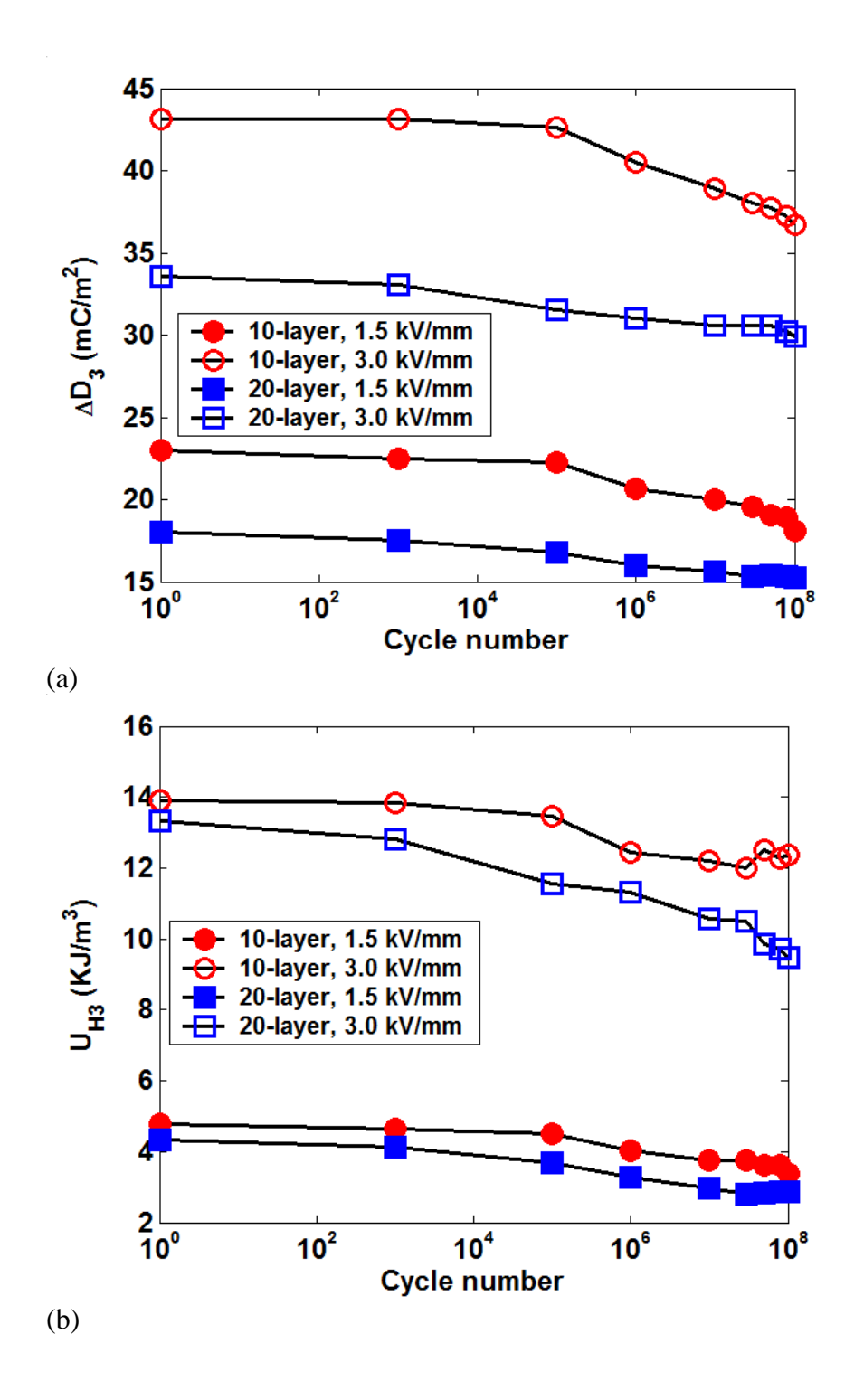


Figure 3(a) Charge density and (b) dielectric hysteresis as a function of cycle number.

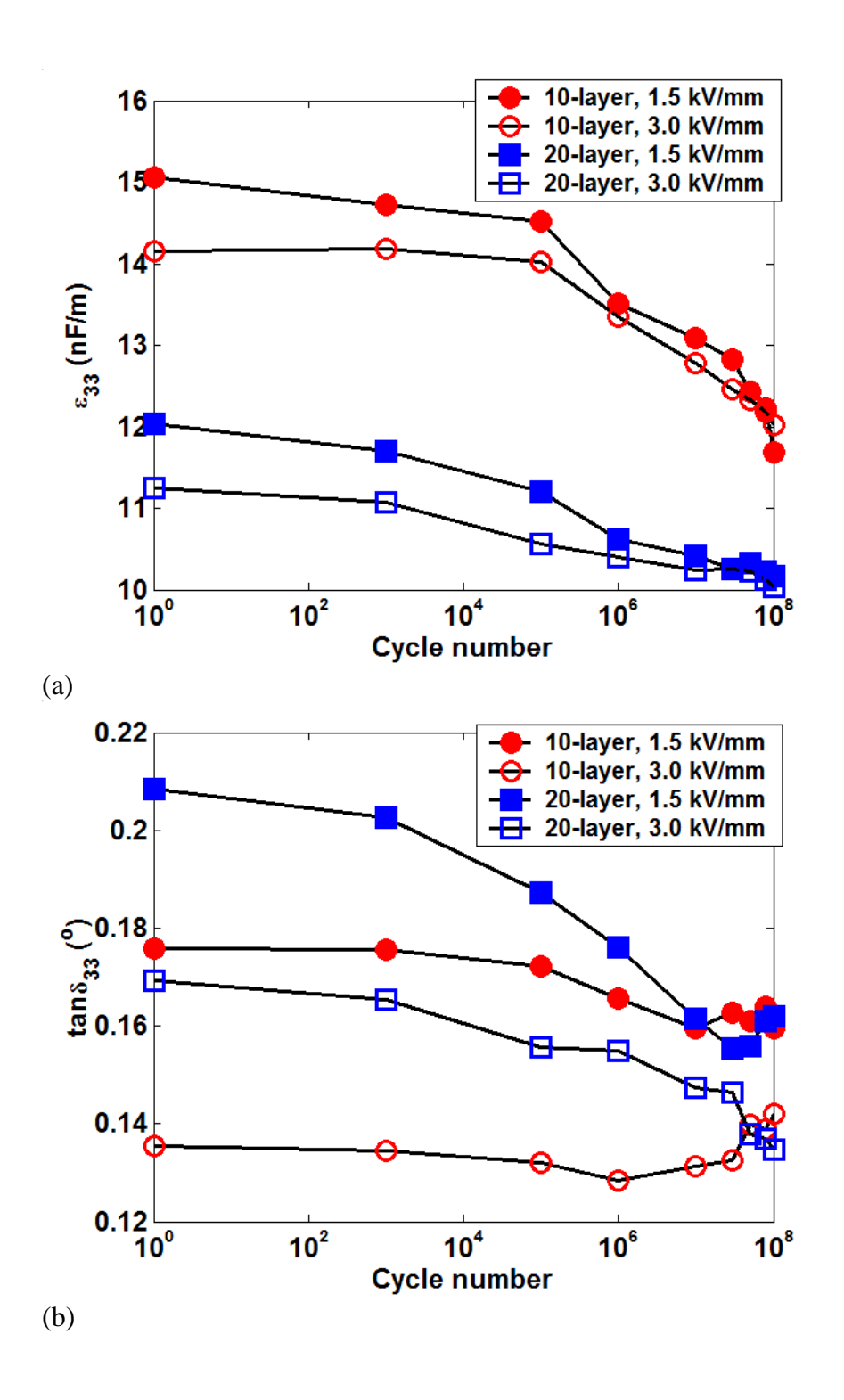


Figure 4(a) Dielectric coefficient and (b) loss tangent as a function of cycle number.

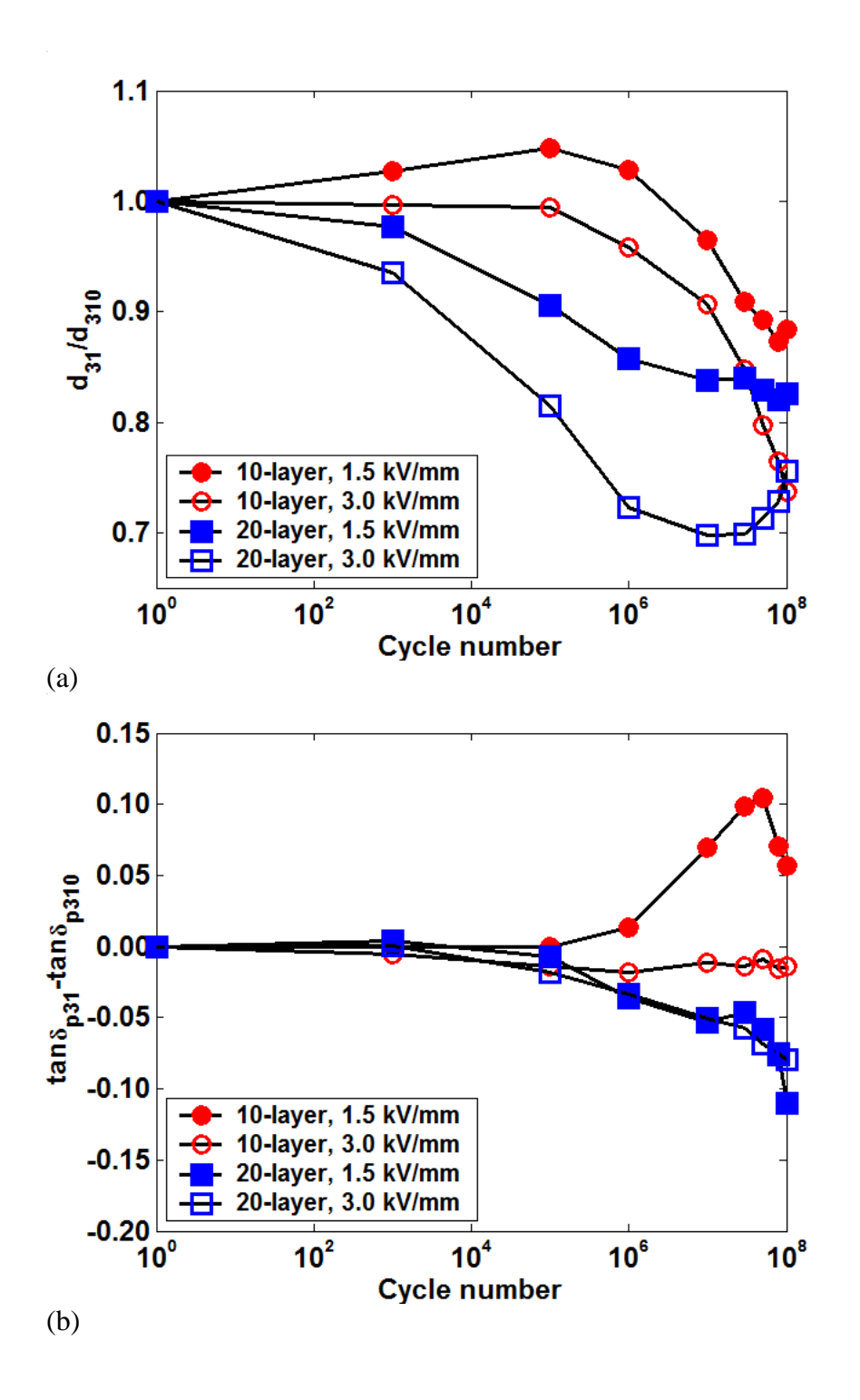


Figure 5(a) Normalized piezoelectric coefficient and (d) shifted piezoelectric loss tangent as a function of cycle number.

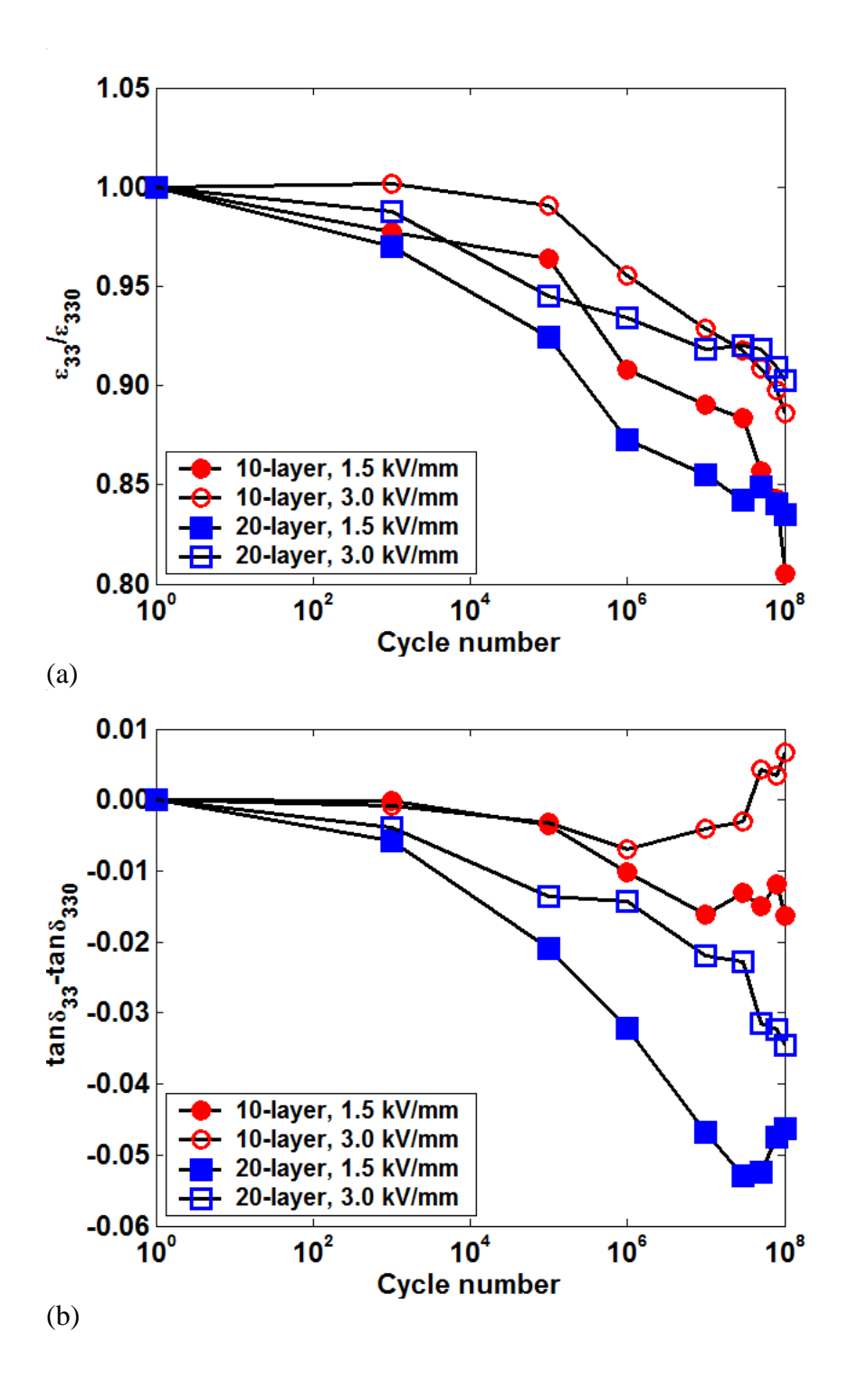


Figure 6(a) Normalized dielectric coefficient and (d) shifted loss tangent as a function of cycle number.

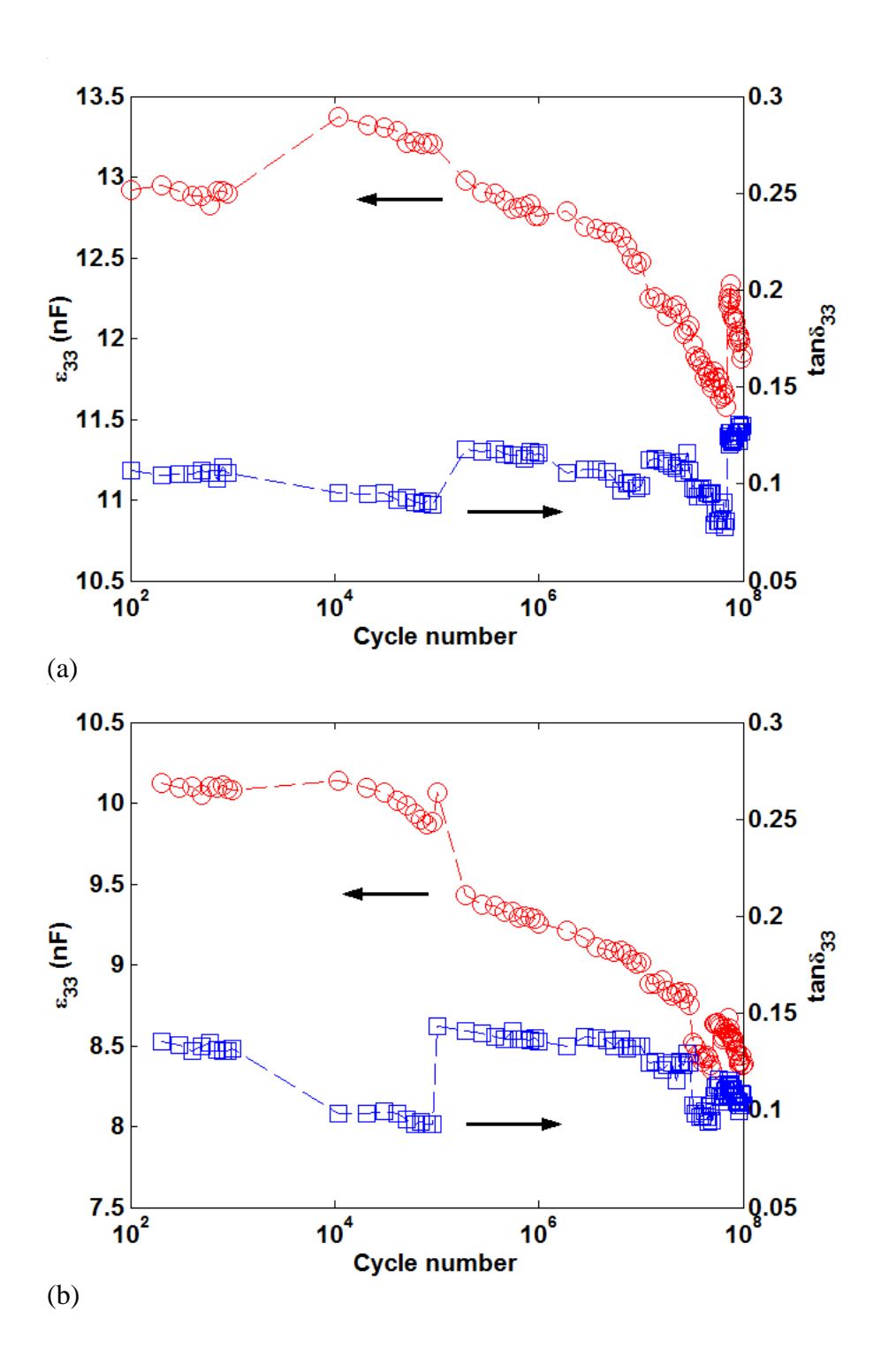


Figure 7 Dielectric coefficient and loss tangent as a function of cycle number based on on-line monitoring for (a) a 10-layer specimen and (b) a 20-layer specimen.

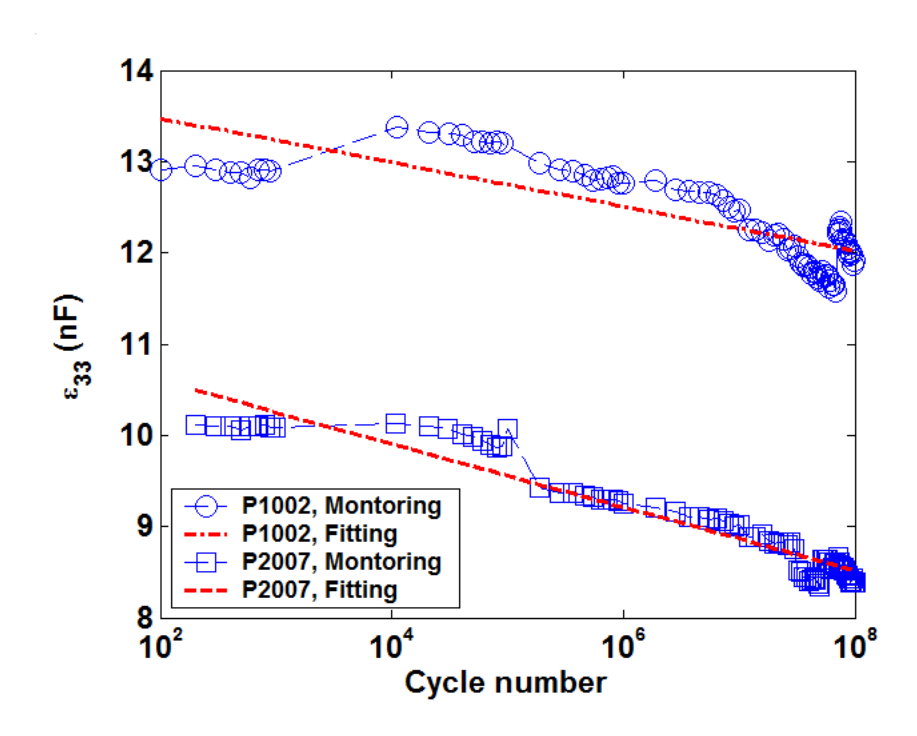


Figure 8 Dielectric coefficient and curve fitting as a function of cycle number based on on-line monitoring for (a) a 10-layer specimen and (b) a 20-layer specimen.

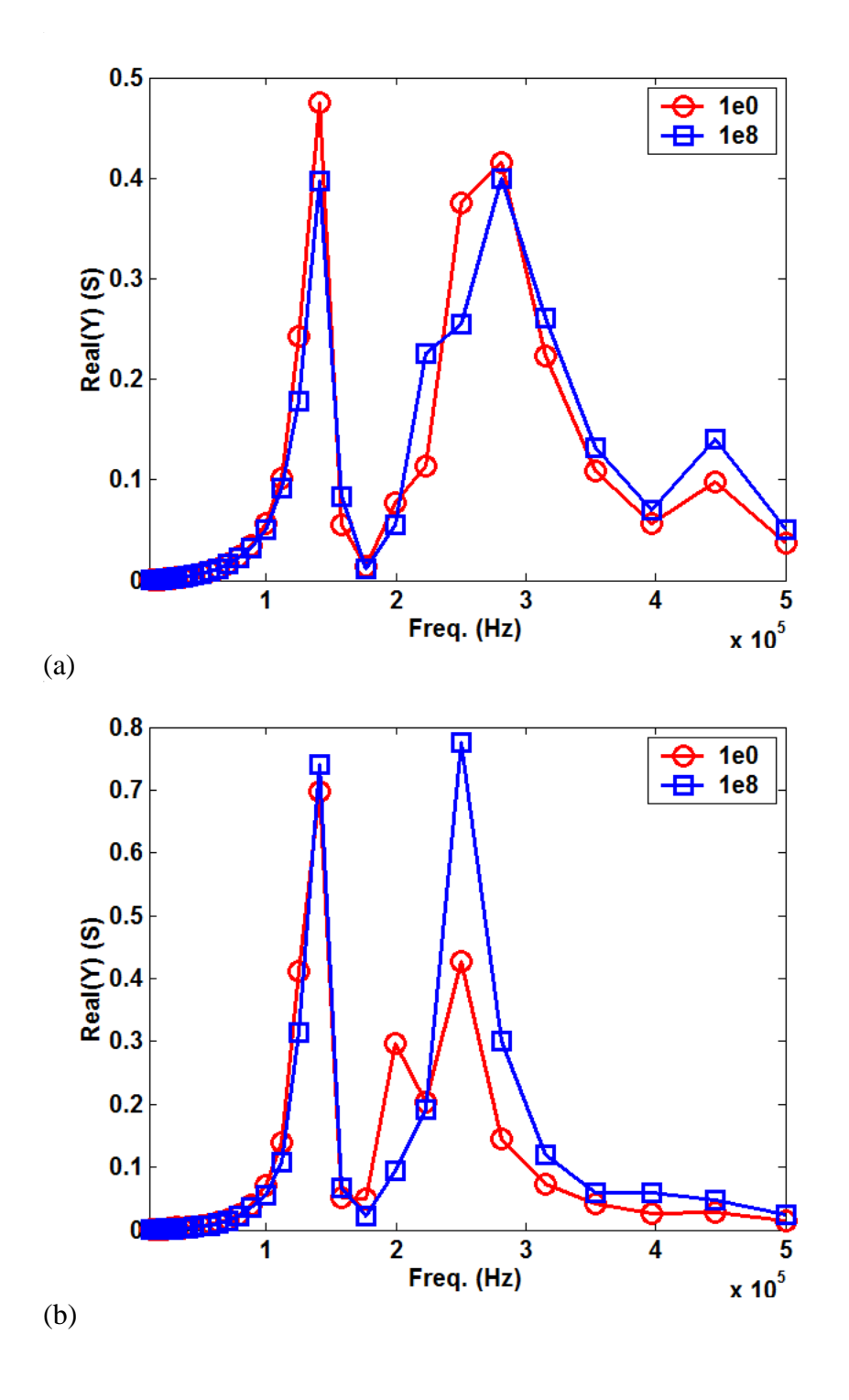


Figure 9 Spectrum of admittance real part (Y) as a function of cycle number for (a) a 10-layer specimen and (b) a 20-layer specimen.

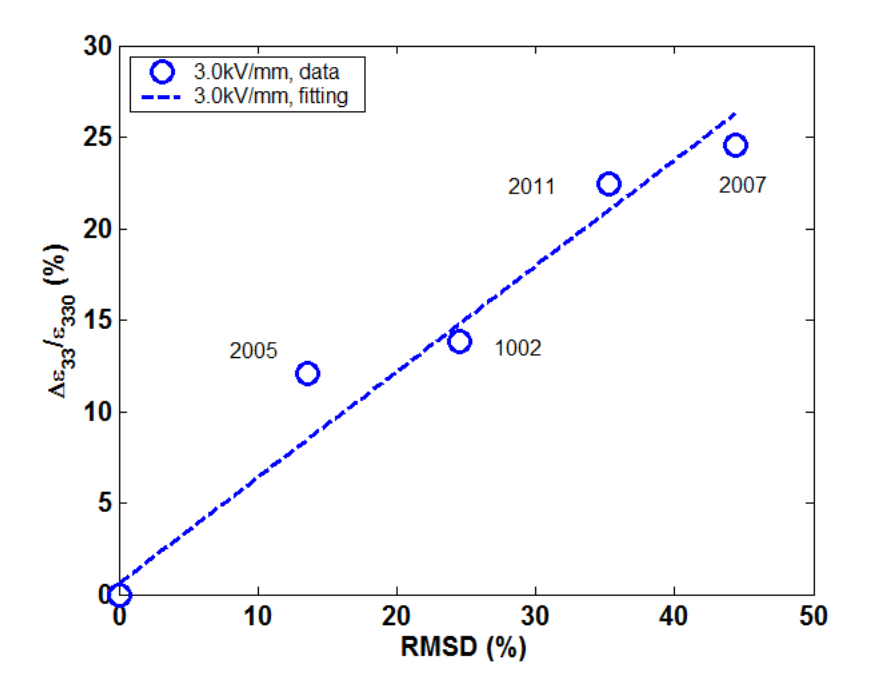


Figure 10 Correlation of relative change of  $\varepsilon_{33}$  to RMSD. Test results are based on on-line monitoring for both 10- and 20- layer specimens.